Quantum Magnetic Skyrmion Operator

Andreas Haller,[1] Sebastián A. Díaz,[2] Wolfgang Belzig,[2] and Thomas L. Schmidt[1]
[1]Department of Physics and Materials Science, University of Luxembourg, 1511 Luxembourg, Luxembourg
[2]Department of Physics, University of Konstanz, 78457 Konstanz, Germany

(Received 18 April 2024; revised 12 July 2024; accepted 15 October 2024; published 22 November 2024)

We propose a variational wave function to represent quantum skyrmions as bosonic operators. The operator faithfully reproduces two fundamental features of quantum skyrmions: their classical magnetic order and a "quantum cloud" of local spin-flip excitations. Using exact numerical simulations of the ground states of a 2D chiral magnetic model, we find two regions in the single-skyrmion state diagram distinguished by their leading quantum corrections. We use matrix product state simulations of the adiabatic braiding of two skyrmions to verify that the operator representation of skyrmions is valid at large interskyrmion distances. Our work demonstrates that skyrmions can be approximately coarse-grained and represented by bosonic quasiparticles, which paves the way toward a field theory of many-skyrmion quantum phases and, unlike other approaches, incorporates the microscopic quantum fluctuations of individual skyrmions.

DOI: 10.1103/PhysRevLett.133.216702

Introduction—Magnetic skyrmions are topologically nontrivial spin configurations that often arise in noncentrosymmetric magnetic materials [1–4] and have mostly admitted a description in terms of classical magnetic moments [5]. However, by now several materials have been found where the sizes of individual skyrmions can be on the order of the spacing of the underlying atomic lattice [6,7]. This makes it necessary to explore their properties based on the underlying quantum mechanical models. Quantum fluctuations, superposition states, and entanglement become unavoidable and fascinating features of quantum magnetic skyrmions that remain largely unexplored despite their relevance for the emerging proposals of skyrmion-based quantum technologies. Such applications include the potential use of skyrmions as qubits in frustrated magnets [8,9] and as mobile impurities to implement topological quantum computing in magnet-superconductor heterostructures [10,11]. The fundamental quantum features of magnetic skyrmions eventually render a classical description unsuitable, hence calling for a new and inherently quantum mechanical theoretical framework.

Quantum magnetic skyrmions emerge, for instance, as the many-body ground state of ferromagnetic spin-1/2 Heisenberg models with either Dzyaloshinskii-Moriya interactions or frustration due to antiferromagnetic next-nearest-neighbor couplings. Since an exact numerical diagonalization of such spin Hamiltonians becomes prohibitive for a large number of lattice sites, the theoretical description of quantum magnetic skyrmions has relied mainly on alternative approaches. Near the classical limit, collective coordinates together with path integral techniques have been employed to model quantum skyrmion nucleation [12,13] and quantum skyrmion dynamics [14,15]. These approaches, unfortunately, are inadequate to model systems of interest for quantum technologies: quantum skyrmions in large numbers and in the deep quantum regime. Here, quantitative predictions for few-skyrmion systems can be made based on exact diagonalization [16–20], neural network states [21,22], dynamical mean-field simulations [23], and density matrix renormalization group simulations [24,25].

In this Letter, we develop a theoretical framework that makes it possible to describe this regime. It is based on the construction of creation and annihilation operators of quantum skyrmions and thus treats magnetic skyrmions as quantum quasiparticles (Fig. 1). This compact and elegant theoretical framework captures the quantum skyrmion's defining features: a classical magnetic order with quantum fluctuations. Constructing this operator allows us to clarify the role played by quantum fluctuations and to determine the range of validity of the semiclassical approximation. The quantum magnetic skyrmion operator is a natural and computationally efficient starting point to model skyrmion-skyrmion interactions and quantum many-body skyrmion phenomena.

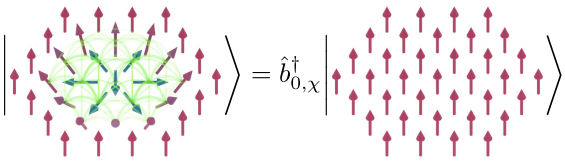

FIG. 1. Creation of a quantum magnetic skyrmion. The quantum magnetic skyrmion operator $\hat{b}^{\dagger}_{0,\chi}$ acts on the field-polarized vacuum state to create a quantum magnetic skyrmion. By construction, the operator captures the fundamental features: classical magnetic order (arrows) and quantum fluctuations visualized by pairwise spin entanglement (green lines).

Quantum skyrmion operator—The quantum skyrmion operator is constructed based on the assumption that a magnetic quantum skyrmion exhibits typical magnetic order in local spin expectation values. This includes cases where the norm of the spin expectation vector is not quantized to the quantum spin s. We focus on $s = 1/2$, but the construction extends to any spin s (see [26], Sec. III). Given the product of local spin rotations,

$$\hat{R}_{\vec{0}}(\boldsymbol{\theta}, \boldsymbol{\phi}) = \prod_{j\neq 0} \mathrm{e}^{-\mathrm{i}\phi_j \hat{S}_{j,z}} \mathrm{e}^{-\mathrm{i}\theta_j \hat{S}_{j,y}}, \tag{1}$$

where site $j = 0$ is excluded, for chosen angles ϕ_j and θ_j, a classical magnetic skyrmion can be expressed as

$$|\Psi_c(\boldsymbol{\theta}, \boldsymbol{\phi})\rangle = \hat{R}_{\vec{0}}(\boldsymbol{\theta}, \boldsymbol{\phi}) \hat{S}_0^- |0\rangle, \tag{2}$$

where $|0\rangle = |\Uparrow\rangle = \otimes_i |\uparrow\rangle_i$ is the vacuum state, and the spin at site $j = 0$ is flipped relative to the polarized environment. Thus, $\hat{b}_{0,0}^\dagger = \hat{R}_{\vec{0}} \hat{S}_0^-$ acts as a creation operator for the classical skyrmion $|\Psi_c\rangle$.

Since $[\hat{R}_{\vec{0}}, \hat{S}_0^-] = 0$, the local commutation relations are $\{\hat{b}_{0,0}, \hat{b}_{0,0}^\dagger\} = 1$ and $[\hat{b}_{0,0}, \hat{b}_{0,0}^\dagger] = 2\hat{S}_{0,z}$. Analogous operators for other sites are $\hat{b}_{i,0}^\dagger = \hat{R}_{\vec{i}} \hat{S}_i^-$. The commutator $[\hat{b}_{i,0}, \hat{b}_{j,0}^\dagger]$ vanishes if sites i and j are sufficiently distant.

To account for quantum fluctuations, we define the quantum skyrmion creation operator,

$$\hat{b}_{i,\chi}^\dagger = \frac{\hat{R}_{\vec{i}}}{\sqrt{\sum_{k=0}^{\chi} |w_k|^2}} \sum_{k=0}^{\chi} w_k \left(\prod_j \left(\hat{S}_j^- \right)^{n_{k,j}} \right), \tag{3}$$

which is the central object of this Letter. $\{w_0, \ldots, w_\chi\}$ are complex scalar weights sorted by descending absolute value, and $\boldsymbol{n}_k$ indicates the number of spin flips. χ is a so-far arbitrary integer that is bounded by the dimension of the Hilbert space. Equation (3) is motivated by the observation that magnetically ordered quantum skyrmion ground states centered at position i are in general surrounded by a "cloud" of spin-flip fluctuations [21,22,24]. For semiclassical skyrmion profiles one has $\boldsymbol{n}_0$ with $n_{0,i} = 1$ and $n_{0,j\neq i} = 0$ associated with the leading contribution $|w_0| > |w_{k\neq 0}|$ from the classical order. The precise form of the other vectors $\boldsymbol{n}_{k\neq 0}$, corresponding to the "quantum cloud," remain undetermined and are model-dependent. It is straightforward to recognize that the local commutation relation of quantum skyrmion operators is approximately given by

$$\left[\hat{b}_{i,\chi}, \hat{b}_{i,\chi}^\dagger\right] \approx \frac{|w_0|^2}{\sum_k |w_k|^2} 2\hat{S}_{i,z}, \qquad \left\{\hat{b}_{i,\chi}, \hat{b}_{i,\chi}^\dagger\right\} \approx \frac{|w_0|^2}{\sum_k |w_k|^2}, \tag{4}$$

together with

$$\left[\hat{b}_{i,\chi}, \hat{b}_{j,\chi}^\dagger\right] = 0 \quad \text{for } |\boldsymbol{R}_j - \boldsymbol{R}_i| > r_c \tag{5}$$

in which r_c denotes the radius of the skyrmion profile. In summary, the quantum skyrmion operator can be interpreted as a bosonic entity with constraints on the local Hilbert space as dictated by the above relations. Using matrix product state simulations, we find the exchange phase is compatible with Eq. (5) (see Appendix). Moreover, the local "hard-core" constraint of Eq. (4) agrees with the numerical observation that many-skyrmion ground states are composed of skyrmion crystals and liquids [24]. The operator can be used to construct a basis of the Hilbert space, referred to as the rotated Fock basis (see [26], Sec. I). The remaining discussion will illustrate for a particular magnetic model how the ratios of the scalar weights w_i/w_0 allow a truncation of the sum to smaller χ values while still approximating low-lying single-particle quantum skyrmion states well using $\hat{b}_{i,\chi}^\dagger |0\rangle$.

Quantum skyrmions in chiral magnets—We investigate a minimal model of a two-dimensional chiral magnet,

$$\hat{H} = \sum_{\langle ij \rangle} \left(\sum_{\alpha=x,y,z} J_\alpha \hat{S}_{i,\alpha} \hat{S}_{j,\alpha} + \boldsymbol{D}_{ij} \cdot \left(\hat{\boldsymbol{S}}_i \times \hat{\boldsymbol{S}}_j \right) \right) + \sum_i \boldsymbol{B} \cdot \hat{\boldsymbol{S}}_i, \tag{6}$$

where $\langle ij \rangle$ denotes a sum over neighboring site pairs (each pair summed once). The three vector components of $\hat{\boldsymbol{S}}_i$ are spin $s = 1/2$ operators, and we assume an interfacial Dzyaloshinskii-Moriya interaction with $\boldsymbol{D}_{ij} = D\hat{e}_z \times \boldsymbol{r}_{ij}/a$, where a is the lattice constant and $\boldsymbol{r}_{ij}$ is the distance vector between neighboring sites.

A system described by Eq. (6) hosts various quantum skyrmion ground states [17,19–21,31,32]. For small systems, finite-size effects are significant, and the properties of low-energy states vary with boundary conditions. Open boundary conditions can lead to helical magnetic spirals, field-polarized states, semiclassical skyrmions, liquids, and lattices. Periodic boundary conditions can yield a symmetric and translation-invariant ground state [17], while a quantum flake in a classical spin field suppresses helical states and removes chiral surface twists [31]. To avoid such boundary effects, we focus on a quantum flake embedded in a fully polarized classical spin field. Given the full lattice $\mathcal{S}$, the quantum spins are on a finite subset $\mathcal{Q} \subset \mathcal{S}$, with $\mathcal{Q} = \{\boldsymbol{R}_i, i = 0, \ldots, N-1\}$, and are described by Eq. (6). We add an environment coupling,

$$\hat{H}_{\mathcal{QC}} = \sum_{\langle ij \rangle} \left(\sum_{\alpha=x,y,z} J_\alpha \hat{S}_{i,\alpha} m_{j,\alpha} + \boldsymbol{D}_{ij} \cdot \left(\hat{\boldsymbol{S}}_i \times \boldsymbol{m}_j \right) \right), \tag{7}$$

where sites j are in the complement $\mathcal{C} = \mathcal{S}\backslash\mathcal{Q}$ and $\boldsymbol{m}_j = (m_{j,x}, m_{j,y}, m_{j,z})$ is a classical spin of length s.

For computational convenience, we use finite triangular lattices with hexagonal C_6 symmetry. We refer to the $N = 7$ flake as a single-shell system and the $N = 19$ flake as a two-shell system, which allows us to investigate small C_6 symmetric quantum skyrmions with a maximal radius $r_c \approx 3a$. While some quantum properties have been explored numerically in larger systems with open boundary conditions [21,24], quantifying quantum fluctuations and their dependence on microscopic parameters remains largely unexplored.

In the next section, we examine skyrmion ground states $|\Psi\rangle$ obtained by exact diagonalization and perform tomography in the rotated Fock basis. This allows us to argue that $|\Psi\rangle \approx \hat{b}^\dagger_{0,\chi}|0\rangle$, where the quality of the approximation is controlled by χ.

Tomography of quantum skyrmions—Using exact diagonalization, we obtain the ground state diagram of Eq. (6) with boundary conditions from Eq. (7), shown in Fig. 2. This diagram is qualitatively similar to previous work [31] but warrants further discussion. Our simulations use 19 sites on a triangular lattice, while previous work used nine sites on a square lattice. Local spin expectation values distinguish three regions: (i) a field-polarized classical state with spin norm $s = |\langle \hat{\boldsymbol{S}}_0 \rangle|$ in the yellow region of Fig. 2(a), (ii) a vortex region with large quantum fluctuations indicated by nearly zero center spin expectation $|\langle \hat{\boldsymbol{S}}_0 \rangle| \approx 0$ and center Rényi entropy $H_{2,0} \approx \ln 2$ in Figs. 2(b) and 2(c), and (iii) a quantum skyrmion regime, shown by contour lines in panels (e) and (f). The quantum skyrmion region is marked by opposite magnetization compared to the field-polarized state [dark blue in Fig. 2(a)] and a finite spin expectation value in panel (b). Field-polarized and quantum

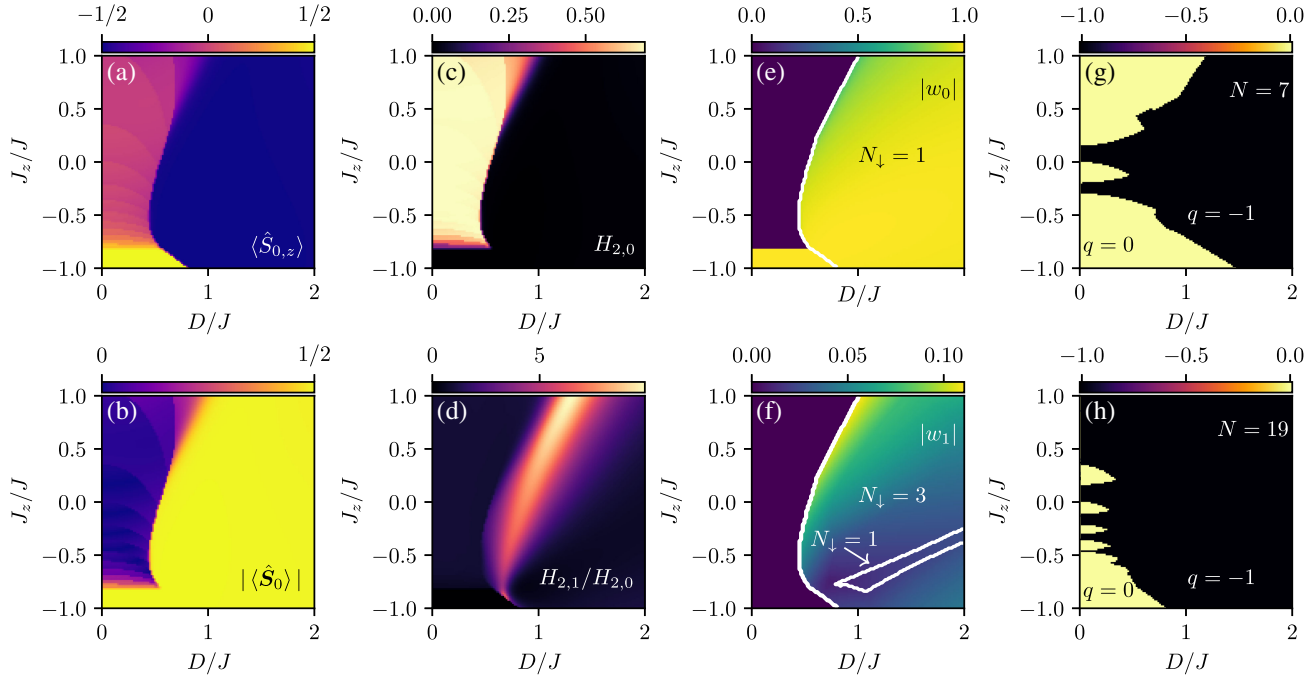

FIG. 2. Quantum magnetic skyrmions and other ground states stabilized in a finite-sized "quantum flake." The quantum flake—a hexagonal region of the lattice of N spins with $s = 1/2$—is part of a chiral magnet embedded in a $m_z = +1/2$ polarized classical environment. The Hamiltonian Eq. (7) models the coupling to the classical environment and Eq. (6) governs the chiral magnet, in which we use a vanishing Zeeman field $B = 0$ and $J_x = J_y = -J$ $(J > 0)$ for the exchange couplings. Varying the Dzyaloshinskii-Moriya interaction amplitude D and the exchange coupling J_z, we use exact diagonalization to compute ground state quantities for $N = 19$ sites: (a) expectation value of the central spin $\langle \hat{S}_{0,z} \rangle$; (b) norm of the central spin $|\langle \hat{\boldsymbol{S}}_0 \rangle|$; (c) center second Rényi entropy $H_{2,0}$; (d) ratio between off-center and center second Rényi entropies $H_{2,1}/H_{2,0}$; probability amplitude magnitudes of the (e) classical magnetic order $|w_0|$ and (f) the six leading quantum corrections with equal amplitudes $|w_1| = |w_2| = \ldots = |w_6|$, defined in Eq. (9), from the ground state expanded in the rotated Fock basis; and (h) topological charge of the ground state magnetization q (defined in [26], Sec. II). In panel (g), we depict q for an $N = 7$ quantum flake. Possible ground states: quantum skyrmion [blue region in (a) where $\langle \hat{S}_{0,z} \rangle \approx -1/2$], field-polarized state [yellow region in (a) where $\langle \hat{S}_{0,z} \rangle = +1/2$], and vortex state [pink region in (a) where $\langle \hat{S}_{0,z} \rangle \approx 0$ with large quantum fluctuations indicated in (c)]. Contour lines and $N_\downarrow = \sum_j n_{k,j}$ in (e) and (f) indicate, respectively, the region and the corresponding number of down spins. In Fig. 3, we show that the $N_\downarrow = 3$ region can be divided into further subregions, distinguished by the distribution of spin flips in the quantum corrections. Probability amplitudes w_0 and w_1 are the weights for constructing the quantum skyrmion operator.

skyrmion states are further distinguished by the ratio of off-center to center Rényi entropy, defined as

$$H_\alpha(\rho_A) = \frac{1}{1-\alpha}\mathrm{tr}\ln(\rho_A^\alpha), \quad \rho_A = \mathrm{tr}_{A^C}|\Psi\rangle\langle\Psi|, \tag{8}$$

where ρ_A is the reduced density matrix for bipartition $A \subseteq \mathcal{Q}$ and the trace is over the complement A^C. In Fig. 2, panels (c) and (d) show the second Rényi entropies for a single-spin bipartition $A_i = \{\boldsymbol{R}_i\}$, i.e., $H_{2,i} = H_2(\rho_{A_i})$. Panel (c) shows $H_{2,0}$ for the center spin, and (d) shows the ratio $H_{2,1}/H_{2,0}$ for an off-center spin $A_1 = \{\boldsymbol{R}_1\}$, $|\boldsymbol{R}_1 - \boldsymbol{R}_0| = a$. Because of the sixfold rotation symmetry, the specific spin choice in the first shell is irrelevant. The ratio $H_{2,1}/H_{2,0}$ in Fig. 2(d) shows that off-center spins are more entangled than the center spin, consistent with larger systems [21,24,33]. Field-polarized states are product states with vanishing Rényi entropy for each spin, while quantum skyrmion states have small but nonzero Rényi entropy. The boundaries between vortex and magnetically ordered states [yellow and blue regions of Fig. 2(b)] shift with system geometry, but qualitative features in the yellow region remain unchanged, indicating minor finite-size effects. In contrast, vortex states in the blue region have near-maximal center site Rényi entropy [in Fig. 2(c)] and almost vanishing spin expectation values. Previous work identified some states in the $q = -1$ lobes of Fig. 2, panels (g) and (h), of the vortex region as quantum skyrmions due to the possibility of defining a quantized topological charge [31]. However, the form of the magnetic profile and the resulting topological charge of the regions with small nonvanishing spin expectations depend strongly on the geometry of the quantum system. We thus focus on a detailed investigation of the unambiguously ordered quantum skyrmion states, for which the quantum skyrmion operator is most relevant. Using the angles associated with the local magnetic order, we expand the wave function in a rotated Fock basis (see [26], Sec. I), and sort the weights by absolute magnitude. These weights can be extracted from the state obtained by exact diagonalization, and are shown in Figs. 2(e),2(f). Depending on the parameters of the system, we find that the ground state wave functions assume two qualitatively different forms, which we denote as $|\Psi_{\mathrm{I},i}\rangle$ and $|\Psi_{\mathrm{II}}\rangle$, i.e.,

$$\begin{aligned}|\Psi_{\mathrm{I},i}\rangle &= \hat{R}_{\bar{0}}\left(w_0|1_0\rangle + w_1\sum_{n=0}^{5}\hat{C}_6^n(|3_i\rangle + e^{i\varphi_i}|3_i'\rangle)\right) + \ldots \\ |\Psi_{\mathrm{II}}\rangle &= \hat{R}_{\bar{0}}\left(w_0|1_0\rangle + w_1\sum_{n=0}^{5}\hat{C}_6^n|1_1\rangle\right) + \ldots,\end{aligned} \tag{9}$$

where we retained the classical magnetic configuration w_0 as well as up to 12 leading quantum corrections w_k with parameter-dependent weights $w_1 = |w_k|$ that can differ by a relative phase φ_i. $\hat{C}_6$ denotes the operator associated with a $\pi/3$ rotation of the Fock state (defined in [26], Sec. I).

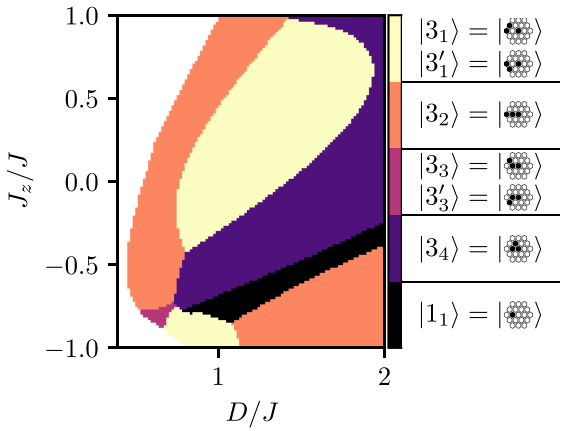

FIG. 3. Regions of different quantum skyrmions, distinguished by their leading quantum corrections [second terms in Eq. (9)]. The Fock states contributing to these corrections are equal up to $\hat{C}_6$ rotations, but differ in the distribution of the down spins, indicated by the graphical notation. States in subregions 2 and 4 do not have mirror-symmetric partner states, i.e., $|3_2'\rangle = |3_4'\rangle = 0$. The black region corresponds to the $N_\downarrow = 1$ region of Fig. 2(f) with states $|\Psi_{\mathrm{II}}\rangle$, and the other regions are subregions of $N_\downarrow = 3$.

The notation $|1_0\rangle$ indicates a state with a single spin down at the center site, $|1_1\rangle$ a state with a spin-down in the first shell surrounding the center, whereas $|3_i\rangle$ and $|3_i'\rangle$ are states with three down spins distributed around and including the center site in four different configurations. The regimes where these different projections contribute to the ground state are presented in Fig. 3.

Notably, the rotated Fock state expansion reveals that the dominant quantum corrections involve only an odd number of down spins, as visible in the $N_\downarrow = \{1, 3\}$ regions of panel (f). More interestingly, the leading quantum corrections can take two qualitatively different forms: the leading quantum corrections in $|\Psi_{\mathrm{I},i}\rangle$ are generated from $N_\downarrow = 3$ states, whereas in $|\Psi_{\mathrm{II}}\rangle$, the leading corrections stem from $N_\downarrow = 1$ states. Therefore, we conclude that the skyrmion phase hosts at least two different types of quantum skyrmions, which have the same classical order but differ in their quantum corrections. Compared to the classical ordered state, the fluctuations in the subleading term of $|\Psi_{\mathrm{I},i}\rangle$ involve flipped spins surrounding the skyrmion center, whereas in $|\Psi_{\mathrm{II}}\rangle$ they include the spin at the skyrmion center and one of its neighboring spins. In Fig. 2, panels (e) and (f), we respectively plot $|w_0|$ and $|w_1|$ together with the associated sum of down spins $N_\downarrow = \sum_j n_{k,j}$. Contour lines mark the domains of different $N_\downarrow$ sectors, where w_0 with $N_\downarrow = 1$ extends over the full skyrmion region in the state diagram. Given that the results reveal only comparatively small quantum fluctuations around an ordered state, on the order of $|w_1/w_0| \sim$ 1–10% [see Fig. 2, panels (e) and (f)], it would be interesting to compare the results presented here with the

outcomes of spin wave theory calculations, in particular magnon squeezed states [34–36].

Finally, we want to highlight that our Fock state expansion could be used as a variational ansatz for the wave function of semiclassical quantum skyrmions, which potentially leads to performant numerical optimization algorithms. The classical magnetic order is captured by two rotation angles per site, resulting in 38 parameters for the 19-site quantum flake that, for the initial state, can be chosen to minimize the classical energy, i.e.,

$$E_c = \min_{\boldsymbol{\theta},\boldsymbol{\phi}} \langle \Psi_c(\boldsymbol{\theta},\boldsymbol{\phi}) | \hat{H} | \Psi_c(\boldsymbol{\theta},\boldsymbol{\phi}) \rangle. \tag{10}$$

In addition to the local order, χ complex weights represent the quantum fluctuations. In the semiclassical skyrmion regime, we recognize from Eq. (9) and Fig. 2, panels (e) and (f), that, by using crystalline symmetries, only two different weights are needed to approximate the quantum mechanical ground state with high fidelity, as the decrease of w_0 is compensated by a simultaneous increase of w_1. The simulation could then be performed by an independent iteration between the optimization of the angles and the weights until convergence is reached. For comparison, we can estimate the number of variational parameters of an unconstrained matrix product state (MPS) simulation. We find that comparable wave function fidelities are reached with bond dimension $M = 3$, which corresponds to MPSs with 302 complex variational parameters. We checked that truncating the Fock state expansion leads to a more efficient representation for bigger skyrmion ground states and higher fidelities as well (see [26], Sec. IV).

Summary and conclusion—In this Letter, we introduced a variational ansatz to represent quantum skyrmions as bosonic operators. The form of this operator is determined by the desire to represent faithfully two fundamentally different aspects of quantum skyrmions: the classical magnetic order and a "quantum cloud" of local spin-flip excitations around the classical magnetic order. Using a minimal model for a chiral magnet in two dimensions, we found two distinct regions in the single-skyrmion phase: one where the leading quantum corrections around the classical magnetic order contain a flip of the center spin and one where they only contain spin flips around the skyrmion center. We argued that the Fock basis of spin flips around the classical order can be particularly useful for numerical algorithms based on the variational principle, because limiting the allowed number of spin flips truncates the dimension of the numerical Fock space and thus reduces the amount of free parameters in the simulations. We expect that such approaches can be fruitful when applied to or combined with tensor network simulations. For this reason, it will be very interesting to investigate quantum skyrmions stabilized by antiferromagnetic frustration with similar techniques as the ones presented in this work. Our work therefore paves the way toward a coarse-grained bosonic description of many-skyrmion quantum phases such as quantum skyrmion liquids that, unlike other approaches, incorporates individual skyrmions' microscopic quantum fluctuations.

Acknowledgments—We thank Alexander Mook, Thore Posske, Matteo Rizzi, Karin Everschor-Sitte, and Niklas Tausendpfund for stimulating discussions. T. .L. S. and A. H. acknowledge financial support from the National Research Fund Luxembourg under Grants No. CORE C20/MS/14764976/TopRel, INTER/17549827/AndMTI, CORE C22/MS/17415246/DeQuSky and AFR/23/17951349. S. D. and W. B. acknowledge funding by the Excellence Strategy of the University of Konstanz via a Blue Sky project and by the Deutsche Forschungsgemeinschaft (DFG, German Research Foundation) via the Collaborative Research Center SFB 1432 Project No. 425217212 and SPP2244 project no. 417034116.

[1] A. Bogdanov and D. Yablonskii, Thermodynamically stable "vortices" in magnetically ordered crystals. The mixed state of magnets, Zh. Eksp. Teor. Fiz. **95**, 178 (1989).
[2] A. Bogdanov and A. Hubert, Thermodynamically stable magnetic vortex states in magnetic crystals, J. Magn. Magn. Mater. **138**, 255 (1994).
[3] U. K. Rößler, A. N. Bogdanov, and C. Pfleiderer, Spontaneous skyrmion ground states in magnetic metals, Nature (London) **442**, 797 (2006).
[4] A. Neubauer, C. Pfleiderer, B. Binz, A. Rosch, R. Ritz, P. G. Niklowitz, and P. Böni, Topological Hall effect in the *A* phase of MnSi, Phys. Rev. Lett. **102**, 186602 (2009).
[5] K. Everschor-Sitte, J. Masell, R. M. Reeve, and M. Kläui, Perspective: Magnetic skyrmions—overview of recent progress in an active research field, J. Appl. Phys. **124**, 240901 (2018).
[6] S. Heinze, K. von Bergmann, M. Menzel, J. Brede, A. Kubetzka, R. Wiesendanger, G. Bihlmayer, and S. Blügel, Spontaneous atomic-scale magnetic skyrmion lattice in two dimensions, Nat. Phys. **7**, 713 (2011).
[7] N. Nagaosa and Y. Tokura, Topological properties and dynamics of magnetic skyrmions, Nat. Nanotechnol. **8**, 899 (2013).
[8] C. Psaroudaki and C. Panagopoulos, Skyrmion qubits: A new class of quantum logic elements based on nanoscale magnetization, Phys. Rev. Lett. **127**, 067201 (2021).
[9] J. Xia, X. Zhang, X. Liu, Y. Zhou, and M. Ezawa, Universal quantum computation based on nanoscale skyrmion helicity qubits in frustrated magnets, Phys. Rev. Lett. **130**, 106701 (2023).
[10] J. Nothhelfer, S. A. Díaz, S. Kessler, T. Meng, M. Rizzi, K. M. D. Hals, and K. Everschor-Sitte, Steering Majorana braiding via skyrmion-vortex pairs: A scalable platform, Phys. Rev. B **105**, 224509 (2022).
[11] S. A. Díaz, J. Klinovaja, D. Loss, and S. Hoffman, Majorana bound states induced by antiferromagnetic skyrmion textures, Phys. Rev. B **104**, 214501 (2021).
[12] S. M. Vlasov, P. F. Bessarab, I. S. Lobanov, M. N. Potkina, V. M. Uzdin, and H. Jónsson, Magnetic skyrmion

annihilation by quantum mechanical tunneling, New J. Phys. **22**, 083013 (2020).
[13] S. A. Díaz and D. P. Arovas, Quantum nucleation of skyrmions in magnetic films by inhomogeneous fields, in *Memorial Volume for Shoucheng Zhang* (World Scientific, Singapore, 2021), Chap. 2, pp. 19–33.
[14] C. Psaroudaki, S. Hoffman, J. Klinovaja, and D. Loss, Quantum dynamics of skyrmions in chiral magnets, Phys. Rev. X **7**, 041045 (2017).
[15] H. Ochoa and Y. Tserkovnyak, Quantum skyrmionics, Int. J. Mod. Phys. B **33**, 1930005 (2019).
[16] V. Lohani, C. Hickey, J. Masell, and A. Rosch, Quantum skyrmions in frustrated ferromagnets, Phys. Rev. X **9**, 041063 (2019).
[17] O. M. Sotnikov, V. V. Mazurenko, J. Colbois, F. Mila, M. I. Katsnelson, and E. A. Stepanov, Probing the topology of the quantum analog of a classical skyrmion, Phys. Rev. B **103**, L060404 (2021).
[18] O. M. Sotnikov, E. A. Stepanov, M. I. Katsnelson, F. Mila, and V. V. Mazurenko, Emergence of classical magnetic order from Anderson towers: Quantum darwinism in action, Phys. Rev. X **13**, 041027 (2023).
[19] V. Vijayan, L. Chotorlishvili, A. Ernst, S. S. P. Parkin, M. I. Katsnelson, and S. K. Mishra, Topological dynamical quantum phase transition in a quantum skyrmion phase, Phys. Rev. B **107**, L100419 (2023).
[20] V. V. Mazurenko, I. A. Iakovlev, O. M. Sotnikov, and M. I. Katsnelson, Estimating patterns of classical and quantum skyrmion states, J. Phys. Soc. Jpn. **92**, 081004 (2023).
[21] A. Joshi, R. Peters, and T. Posske, Ground state properties of quantum skyrmions described by neural network quantum states, Phys. Rev. B **108**, 094410 (2023).
[22] A. Joshi, R. Peters, and T. Posske, Quantum skyrmion dynamics studied by neural network quantum states, Phys. Rev. B **110**, 104411 (2024).
[23] R. Peters, J. Neuhaus-Steinmetz, and T. Posske, Quantum skyrmion Hall effect in f-electron systems, Phys. Rev. Res. **5**, 033180 (2023).
[24] A. Haller, S. Groenendijk, A. Habibi, A. Michels, and T. L. Schmidt, Quantum skyrmion lattices in Heisenberg ferromagnets, Phys. Rev. Res. **4**, 043113 (2022).
[25] Z. Zhao, E. Östberg, F. Aryasetiawan, and C. Verdozzi, Quantum magnetic skyrmions on the Kondo lattice, arXiv:2405.20897.
[26] See Supplemental Material at http://link.aps.org/supplemental/10.1103/PhysRevLett.133.216702 where we discuss details of the rotated Fock state basis, fidelity, topological charge, and adiabatic exchange of two semiclassical skyrmions, which includes Refs. [27–30].
[27] A. Perelomov, *Generalized Coherent States and Their Applications*, Theoretical and Mathematical Physics (Springer, Berlin, Heidelberg, 2012).
[28] B. Berg and M. Lüscher, Definition and statistical distributions of a topological number in the lattice o(3) sigma-model, Nucl. Phys. **B190**, 412 (1981).
[29] X. S. Wang, H. Y. Yuan, and X. R. Wang, A theory on skyrmion size, Commun. Phys. **1**, 31 (2018).
[30] M. B. Hastings, An area law for one-dimensional quantum systems, J. Stat. Mech. (2007) P08024.
[31] P. Siegl, E. Y. Vedmedenko, M. Stier, M. Thorwart, and T. Posske, Controlled creation of quantum skyrmions, Phys. Rev. Res. **4**, 023111 (2022).
[32] F. Salvati, M. I. Katsnelson, A. A. Bagrov, and T. Westerhout, Stability of a quantum skyrmion: Projective measurements and the quantum Zeno effect, Phys. Rev. B **109**, 064409 (2024).
[33] D. Bhowmick, A. Haller, D. S. Kathyat, T. L. Schmidt, and P. Sengupta, Quantum skyrmion liquid, arXiv:2407.10637.
[34] A. Kamra, E. Thingstad, G. Rastelli, R. A. Duine, A. Brataas, W. Belzig, and A. Sudbø, Antiferromagnetic magnons as highly squeezed Fock states underlying quantum correlations, Phys. Rev. B **100**, 174407 (2019).
[35] K. Mæland and A. Sudbø, Quantum fluctuations in the order parameter of quantum skyrmion crystals, Phys. Rev. B **105**, 224416 (2022).
[36] K. Mæland and A. Sudbø, Quantum topological phase transitions in skyrmion crystals, Phys. Rev. Res. **4**, L032025 (2022).
[37] M. V. Berry, Quantal phase factors accompanying adiabatic changes, Proc. R. Soc. A **392**, 45 (1984).
[38] C. Nayak, S. H. Simon, A. Stern, M. Freedman, and S. Das Sarma, Non-Abelian anyons and topological quantum computation, Rev. Mod. Phys. **80**, 1083 (2008).
[39] R. A. Istomin and A. S. Moskvin, Overlap integral for quantum skyrmions, J. Exp. Theor. Phys. Lett. **71**, 338 (2000).

End Matter

Appendix: Exchange angle—One characteristic quantity related to the elementary form of a quantum mechanical many-body wave function is the statistical phase after particle exchange. A wave function of two bosons (fermions) $\Psi(\boldsymbol{x}_1,\boldsymbol{x}_2)$, with $\boldsymbol{x}_1 \neq \boldsymbol{x}_2$ the different positions of two identical particles, acquires a statistical phase $+1$ (-1) after particle exchange $\Psi(\boldsymbol{x}_1,\boldsymbol{x}_2) \to \Psi(\boldsymbol{x}_2,\boldsymbol{x}_1) = \pm\Psi(\boldsymbol{x}_1,\boldsymbol{x}_2)$. The exchange phase can be understood geometrically through the Berry phase [37,38]. To compute the Berry phase, we add to the Hamiltonian in Eq. (6) of the main text the following pinning potential:

$$\hat{V}(\lambda) = V_0 \sum_{j=1}^{N} \sum_{i=1}^{2} \exp\left(-\frac{|\boldsymbol{R}_j - \boldsymbol{x}_i(\lambda)|^2}{2\sigma^2}\right) \hat{S}_{z,j}. \tag{A1}$$

In the resulting Hamiltonian $\hat{H}(\lambda)$, if the exchange couplings are tuned such that the ground state is polarized to the external field, using $V_0 \gg J$ pins exactly two semiclassical skyrmion profiles around the center-of-mass positions $\boldsymbol{x}_1(\lambda)$ and $\boldsymbol{x}_2(\lambda)$. Smoothly deforming the pinning potential so that $\boldsymbol{d}(\lambda) \coloneqq \boldsymbol{x}_2(\lambda) - \boldsymbol{x}_1(\lambda)$ rotates by π in the interval $\lambda \in [0,1]$ defines a closed path in the parameter space of $\hat{H}(\lambda)$

where the two identical skyrmions exchange positions. Suppose $\lambda(t)$ is changed adiabatically in time. In that case, we can assume that the ground state $|\Psi\rangle$ follows the parameter deformation instantaneously, such that $|\Psi(t)\rangle = |\Psi[\lambda(t)]\rangle$.

For skyrmion profiles with radius $r_c \approx 3a$, a well-separated two-skyrmion magnetization profile already requires system sizes that cannot be investigated by exact diagonalization. Instead, we proceed by using MPS simulations for larger quantum systems, which are known to faithfully capture the properties of quantum skyrmion ground states [24,33]. The Berry phase is then extracted by (i) using variational MPS to evaluate the ground states of a discrete sequence in the adiabatic deformation loop, i.e., $\{|\Psi_n\rangle \coloneqq |\Psi(n\Delta\lambda)\rangle, n = 0, \ldots, N_\lambda - 1\}$ with $\Delta\lambda = 1/N_\lambda$, and (ii) evaluating the Berry phase through a Wilson loop,

$$\phi = \arg \prod_n \frac{\langle \Psi_n | \Psi_{n+1} \rangle}{|\langle \Psi_n | \Psi_{n+1} \rangle|}, \tag{A2}$$

where $|\Psi_{N_\lambda}\rangle = |\Psi_0\rangle$. It is easy to recognize that the Berry phase ϕ obtained by the Wilson loop is invariant under gauge transformations $|\Psi_n\rangle \to e^{i\varphi_n}|\Psi_n\rangle$ by definition, as every state occurs exactly twice in ϕ, thereby canceling the arbitrary complex phase φ_n, such that we do not need to fix a gauge for the numeric simulations. We deform the skyrmion along a C_6 hexagonal path and the distance d is defined as the diagonal of the hexagon. The adiabatic sequence is chosen along the six lines forming the path, with a discretization step of $a/8$ that guarantees sufficiently large wave function overlaps $|\langle \Psi_n | \Psi_{n+1} \rangle| \geq 0.86$ for all simulations. To embed the two-skyrmion state in a sufficiently large polarized environment, we perform simulations on a rhomboid grid of size $L_1 = L_2 = d + 11a$ (from 17×17 to 23×23) with the boundary conditions of Eq. (7). In Fig. 4 panel (a), we depict some spin expectation values from the adiabatic sequence of $d = 6a$. For a given set of MPS parameters, 72 (for $d = 6a$), 96 ($8a$), 120 ($10a$), and 144 ($12a$) individual simulations approximate the ground states that form the overlap elements of the Wilson loop.

Memory constraints limit the possibility of running these simulations in parallel, and long run times result from a slow energy convergence: between 100 and 1000 sweeps are needed to converge the energy up to the 12th significant digit—the chosen criterion after which the simulations are stopped. The system parameters for the braiding protocol are thus deliberately chosen so that the quantum skyrmion states carry weak quantum fluctuations. This allows us to reach high-fidelity approximations at moderate computational effort, i.e., up to a maximum bond dimension $M = 256$. The exchange angle ϕ, numerically computed at various skyrmion separations d, is shown in Fig. 4. Although the simulations overestimate the true exchange angle, we find a

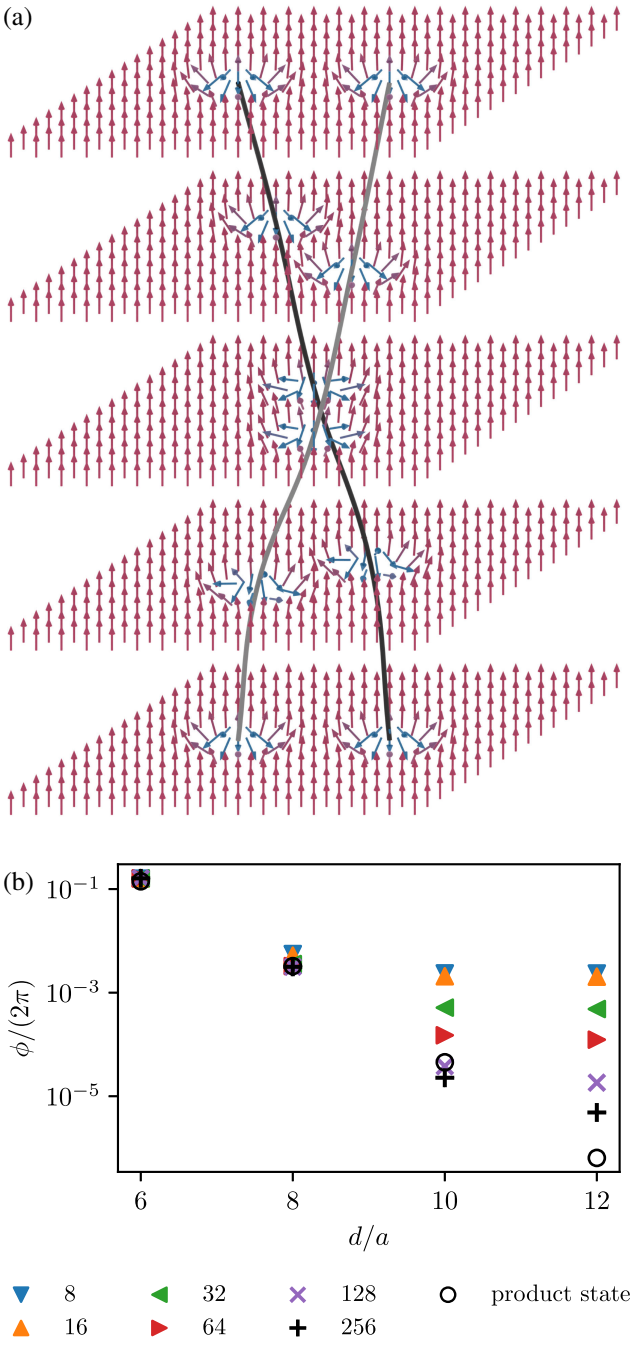

FIG. 4. Panel (a) visualizes the braid of two quantum skyrmions by a deformation of the pinning potential for $d = 6a$. The result of the exchange angle for different d (system sizes are 17×17, 19×19, 21×21, and 23×23) is shown in (b), for $V_0 = 4J$, $J_x = J_y = J_z = -J = 0.3D$, $\sigma = a$, and $\boldsymbol{B} = 2D\boldsymbol{e}_z$ and different bond dimensions M (triangles and crosses). We recognize that $M \to \infty$ approaches an exponentially vanishing trend in the distance d, compatible with an approximately bosonic two-skyrmion wave function. A product state approximation (black circles) of two classical skyrmions quantitatively recovers the exponential trend of the exchange angle on large distances. On short distances, differences are caused by quantum fluctuations surrounding the skyrmion core.

trend compatible with an exponential decay—most strikingly revealed by a product state approximation of the two-skyrmion state (black circles in Fig. 4). The numerical results thus demonstrate the feasibility of Eq. (3) with a strongly truncated χ ($\chi = 1$ for product states), and the bosonic nature of quantum skyrmions at distances $\gtrsim 2r_c$.

On large distances, interskyrmion interactions are negligible and one may apply Eq. (3) for the individual entities, clearly exhibiting the bosonic algebra of Eq. (5). It is reasonable to argue that the two skyrmions behave as bosonic quasiparticles, provided they are separated over large distances.

On short distances comparable with the skyrmion radius $d \sim 2r_c$, the exchange phase does not vanish, which is expected because the rotation operators associated with the classical magnetic order overlap [39].